

Using CFD-Based Virtual Sensor Data to Study the Structure of Air Flow behind A Porous Fence

Yizhong Xu and Mohamad Y. Mustafa

Atmospheric Icing Research Team

Narvik University College

Narvik, Norway

Yizhong.Xu@hin.no and MohamadYazidF.Mustafa@hin.no

Abstract— Physical experiments have difficulties to thoroughly investigate the full structure of air flow behind a porous fence. Physical measurement sensors have their limitations of data acquisitions in turbulent air flow. Computational Fluid Dynamics (CFD) technique provides an infinite number of virtual sensors that allows producing quantitative CFD-based virtual sensors data for users. In this paper, a 3D CFD model is assessed by the physical sensors data, and the simulation has provided comprehensive information for studying the structure of airflow in a 3D domain.

Keywords—physical sensor; virtual sensor; wind tunnel experiment; 3D CFD model; CFD-based virtual sensor data

I. INTRODUCTIONS

In cold regions like Norway, the outdoor environment can be extremely hostile towards human activities. Porous fence is one of common devices widely applied in these regions. It serves as windbreaks to effectively mitigate the damages caused by strong wind and transported sediments. Therefore it can create an operable and habitable space for human needs.

The structure of air flow behind a porous fence is complex due to the presence of the bleed flow passing through the pores in the fence and the displaced flow passing over the fence. Figure 1. shows a comparison of flow regimes behind porous fences as porosity above and under critical porosity, where β is porosity of fence, and β_{crit} is critical porosity of fence.

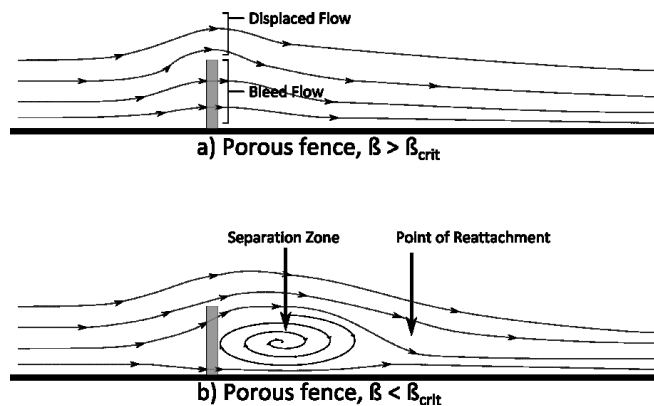


Figure 1. Comparison of flow regimes behind porous fences as porosity approaches critical porosity

Critical porosity β_{crit} is defined as the maximum fence porosity below which flow separation and reversal occurs [1]. Above the critical porosity, the airflow in the leeward is dominant by bleed flow and there is no flow separation (Figure1, a). Below the critical porosity, the leeward airflow directly behind the fence reverses, resulting in a region of recirculating air (Figure1, b). In general, fence porosity in the range of 0.20-0.50 is considered to give noticeable changes of flow structures behind fences [2] [3] [4] [5].

Physical experiments to investigate the structure of air flow behind porous fences are quite challenging, due to the presence of turbulence. Conventional cup-type anemometer is the earliest device to give a rough estimate of turbulence intensity in the field tests [6]. Hot-Wire anemometer (HWA) and Pulsed-Wire anemometer (PWA) must be positioned at specific measurement points to obtain results, that will distort the airflow field. Laser Doppler anemometer (LDA) and Phase Doppler anemometer (PDA) are non-intrusive to the measured airflow field. However, like HWA and PWA, LDA and PDA only provide time-averaged velocity and turbulence intensity values at discrete measuring points, and have difficulties to measure the near-wake regions behind fences. Particle Image Velocimetry (PIV) and Particle Tracking Velocimetry (PTV) as recently developed non-intrusive measurement techniques can obtain instantaneous velocity measurements and are related properties in a target area. The air is seeded with tracer particles, which must be sufficiently small to be assumed to faithfully follow the air dynamics. In practice, PIV and PTV are costly, and usually are not applied in field measurements. Overall, the above physical sensors have their limitations, and have difficulties to obtain a high-resolution data set within a space of airflow influenced by a porous fence.

Over the last three decades, with the rapid development of computer technology and Computational Fluid Dynamics (CFD) techniques, numerical simulation has been increasingly employed in porous fence researches. Wilson[7] introduced a momentum sink involving the fence resistance coefficient to simulate a porous fence solved by Reynolds-averaged Navier-Stokes (RANS) equation. His results demonstrated a promising prediction in terms of the flow structure around the fence. Under different fence porosities and different turbulence models, Packwood [8]

examined numerical results against wind tunnel experimental results through a 2D thin fence model in a thick boundary layer. He found that the k-ε incorporated a Preferential Dissipation Modification (PDM) model worked better. Bourdin and Wilson [10] confirmed the suitability of CFD with regard to windbreak aerodynamics, based on the comparison of the numerical data (2D and 3D model simulation) against the experimental data. Alhajraf [9] introduced a CFD model for 2D and 3D simulations of drifting particles at porous fences. His model showed good agreement with the field observations and the wind tunnel measurements.

Virtual sensor is a smart sensor, it can be used for computing estimating complex variables that otherwise should require very expensive equipment or laboratory tests [11]. Recently CFD-based virtual sensor data as alternatives to physical sensor data are increasingly adapted by researchers. Jang et al. [12] implemented CFD-based virtual sensor data in a micro-scale air quality management system. Sun and Wang [13] used CFD-based virtual sensor data to control indoor environment and space ventilation.

In this paper, a porous fence with porosity of 0.23 has been selected for the case study that ensures recirculating air occurred in the flow regime behind the porous fence. Section 2 is the theoretical framework discussed about the novelty and robustness of the CFD-based virtual sensor data. Section 3 and Section 4 are the case study carried out in physical wind tunnel and virtual wind tunnel (numerical), where the detailed procedures of physical test and numerical simulation are presented. In Section 5, the 3D CFD model has been assessed against wind tunnel experiment, and the simulation results have been demonstrated and discussed. Finally, the capability of CFD-based virtual sensor data to study the structure of airflow behind a porous fence has been concluded in Section 6.

II. THEORETICAL FRAMEWORK

Blocken [14] reviewed a perspective on the past, present, future of Computational Wind Engineering (CWE), and made a statement: “CFD offers some particular advantages compared with on-site measurements and reduced-scale wind tunnel measurements. They can provide detailed information on the relevant flow variables in the whole calculation domain, under well-controlled conditions and without similarity constraints.” CFD technique is an efficient, flexible and relatively cheap alternative to physical experiment that has been widely recognized in the porous fence research industry nowadays. Effective application of CFD is the combination of knowledge in domain physics and numeric. When adequate physical models are selected and supplied with the correct data, essentially, CFD allows for an infinite number of virtual sensors to assess the performance of a unit.

Reynolds-averaged-Navier-Stokes (RANS) equations are the most popular governing equations to describe turbulence

flow behind porous fences so far, which are mathematically expressed as follows:

$$\frac{\partial u_j}{\partial x_j} = 0 \quad (1)$$

$$\frac{\partial u_i}{\partial t} + u_j \frac{\partial u_i}{\partial x_j} = -\frac{1}{\rho} \frac{\partial p}{\partial x_i} + \frac{\mu}{\rho} \frac{\partial^2 u_i}{\partial x_i \partial x_j} - \frac{\partial}{\partial x_j} (\overline{u'_i u'_j}) + g_i \quad (2)$$

where u_j is the j component of velocity, t is the time, x_j is the j coordinate, ρ is the air density, μ is the dynamic viscosity, and g_i is the gravitational body force.

The RANS are time-averaged equations of motion for airflow that need to solve a closure problem because of the non-linear term from the convective acceleration, known as the Reynolds stress. For the porous fence research, k-Epsilon and k-Omega are the two most popular turbulence closure models used in CFD simulations [7] [8] [15] [16]. The main difference between them is that k-Epsilon model solves kinetic energy and turbulence dissipation, while the k-Omega model solves kinetic energy and turbulence frequency. Although it is well acknowledged that the selection of turbulence models is sensitive to the accuracy of numerical results, the suitability of turbulence models varies individually. It is still open to debate the issue of turbulence model selections in the research field.

The main limitation of RANS modeling is incapable to simulate the inherently transient features of the airflow field such as separation and recirculation downstream of windward edges and vortex shedding in the wake. Large-eddy simulation (LES) can explicitly resolve these large-scale features. However, LES increases computational requirements and has the difficulty in specifying appropriate time-dependent inlet and wall boundary conditions. Nevertheless, mathematical model based on the RANS equations has been used successfully for studies of the structure of airflow behind porous fences.

CFD simulation provides virtual sensor data to estimate product properties or process conditions based on mathematical models. These mathematical models use other physical sensor readings to calculate the estimations. Inlet velocity profile and boundary conditions are those of physical sensor data that will be introduced into the mathematical model as the pre-set data, which reflects to the real scenario. Consequently, CFD simulation creates a channel through which a virtual system (CFD-based virtual sensor data) has communicated with a natural system (physical sensor data and empirical knowledge) in a way that improves understandings for researchers.

Care for high quality and reliability of CFD simulations is crucial. Numerical and physical modeling errors must be assessed. Without validation against physical experiments, the robustness of CFD-based virtual sensor data is questionable.

III. CASE STUDY SETUP

The physical experiment for this case was conducted in a closed return wind tunnel at Narvik University College. A porous fence was placed at the center of the cross section of the wind tunnel with a distance of 1000mm from the leading edge of the test section (upstream). The configuration of the fence is 650mm width * 200mm height * 3mm thickness, and it is oval holed with porosity of 0.23 . The CFD simulation domain was configured by the exact size of the physical domain, which makes the 3D domain with dimensions: 655mm height, 4000mm length and 1160mm its maximum width. Figure 2 shows the physical wind tunnel experiment setup. Figure 3 displays the 3D virtual wind tunnel domain.

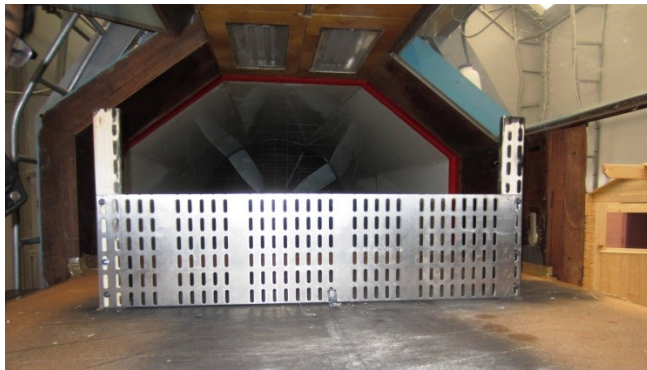


Figure 2. Physical wind tunnel experiment setup

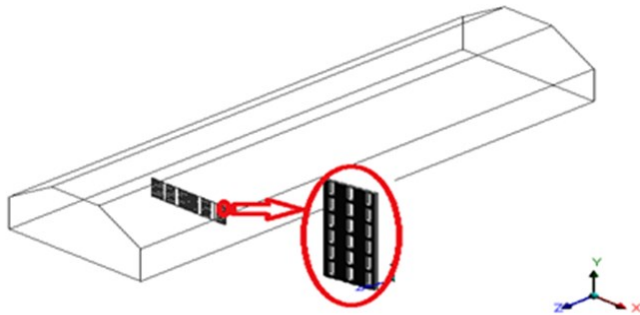


Figure 3. 3D virtual wind tunnel simulation domain

The physical wind tunnel experiment is designed to investigate the structure of airflow behind the fence under free upstream velocities of 15m/s and 20m/s respectively. A Pitot static tube was placed at the entrance of the test section to monitor the upstream velocities, and a traverse attached with a Hot-Wire Anemometer (HWA) was positioned at a longitudinal distance of 925mm downstream of the fence. Test data were taken by moving the traverse at steps of 0.2 inch in the vertical direction. To improve the accuracy of the data, 50 readings have been taken for each step, and then time averaged data were recorded.

The physical experiment revealed the inlet velocity profiles were fully developed and obeyed the power law profile:

$$u = U_{free}(y/\delta)^\alpha \tag{3}$$

Where the U_{free} is the free stream inlet velocity which is measured 15m/s and 20m/s here respectively. δ is the boundary layer thickness which is equal to 10mm . The exponent α is 0.11 .

Equation (3) was written in program C language and was interpreted into the CFD model. As such, the real sensor data have been transferred into the numerical simulations.

IV. NUMERICAL SIMULATION

The CFD simulations were performed under ANSYS 14.0 Fluent workbench package. To optimize resources the meshed domain was reduced down to half since it was symmetrical in the YZ plane and an air box (length * width * height = $3000\text{mm} * 400\text{mm} * 300\text{mm}$ with the upstream length of 500mm) was created to dense the elements around the fence. Figure 4 demonstrates the creation of the CFD domain and its meshed symmetry wall.

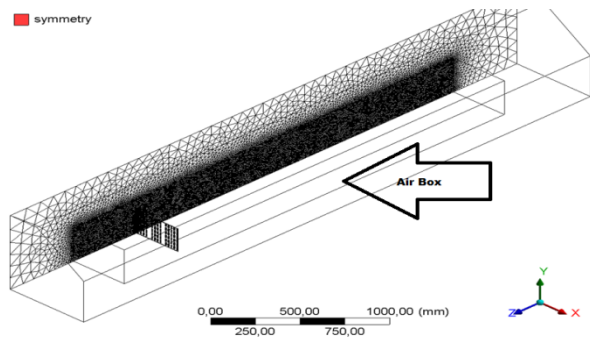


Figure 4. CFD domain & its meshed symmetry wall

In this paper, realizable k-Epsilon turbulence model with Non-Equilibrium Wall Function is employed, as it is in remarkable agreement with the considerable testing results [17].

Mesh sensitivity study was carried out under the same simulation conditions, where tetrahedral and polyhedral elements have been performed through 6 different meshing scales. The parameters selected to check the mesh independent condition of grid were velocity magnitudes and turbulent kinetic energies (TKEs). It was examined that the mesh with 6.3 million tetrahedral elements was desirable.

Turbulent intensity ratio and viscosity ratio were set at 1% and 10% respectively after the inlet velocity profiles were hooked. The gauge pressure at the pressure outlet was set at 0 Pascal with the backflow turbulent intensity ratio and viscosity ratio as 5% and 10% . All of the rest boundary conditions were treated as no-slip stationary wall with 1mm roughness height and 0.5 roughness constant. The solution method was the pressure-velocity coupling the Semi-Implicit Method for Pressure-Linked Equation (SIMPLE) scheme, since the scheme has been extensively used for atmospheric flows [16] [17].

The convergence criteria were set the scaled residuals below $1 \cdot 10^{-4}$, and mass flow rates between velocity inlet and pressure outlet have been checked afterwards.

V. RESULTS AND DISCUSSIONS

A. Assessment of 3D CFD model

The comparisons of velocity magnitudes between the numerical and experimental results is presented in Figure 5, where H/h is the ratio of the measuring height to the fence height. The acquired data were taken along a vertical line $925mm$ downstream of the fence in the symmetry wall, which is correspondent to the exact position of the experimental measurement line.

Comparisons among CFD and experimental results

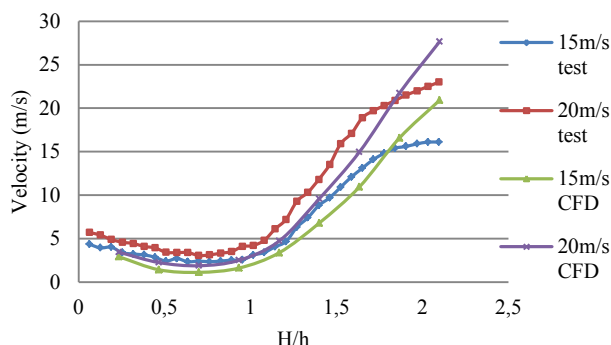


Figure 5. Comparisons between CFD and wind tunnel results

It is observed that the numerical results are in good agreement with the experimental results especially within the range of $H/h = 1.2$. Beyond the range of $H/h = 1.8$, velocity magnitude in the CFD grows faster than that in the experiment. The reason can be attributed to the fact that the blockage ratio of the wind tunnel in the current setting is 9.8%. It is slight high that increases the effects of the top wall boundary layer on the regional velocities in the physical test, while for the case of CFD, the roughness height of the top wall is set to $1mm$.

The CFD simulation over-predicted the reduction of velocity when compared to the physical measured results. In general, it is describable.

B. Domain structure of air flow

The 3D CFD simulation provides an infinite number of virtual sensor data to form a comprehensive structure of air flow in the targeted domain. It allows assessing the performance of any unit. Figure 6 and Figure 7 display the contours of velocity magnitude and kinetic energy respectively, where the free stream velocity is at $20m/s$, plane-1 is parallel to the symmetry wall with $x = 11mm$, plane-2 is parallel to the floor with $y = 0mm$, and plane-3 is parallel to the velocity inlet with $z = 1500mm$. The domain structure of air flow is agreed to the descriptions of other researchers [1] [18].

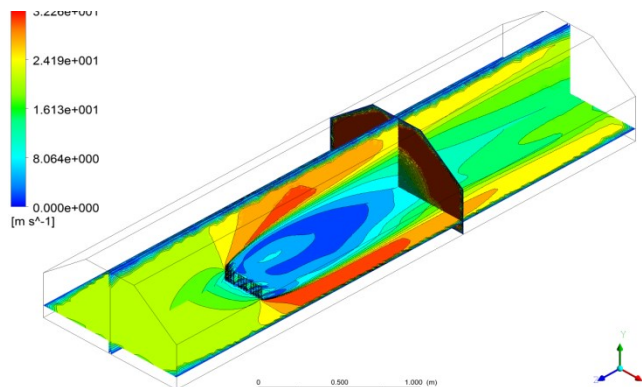


Figure 6. Velocity magnitude contours in the 3 planes

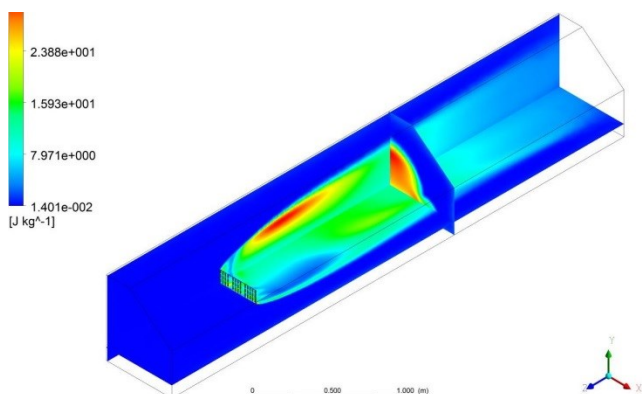


Figure 7. TKE contours in the 3 planes

C. Shear stress distributions in fence porous zone

One of advantages in 3D CFD simulation is that it allows scrutinizing shear stress and pressure distributions in porous fence zone. Unlike 2D model, 3D model can directly reflect this information in detail without modifying momentum and inertial loss within the porous zone. Figure 8 shows the shear distribution in the porous zone. These data are not possible to be obtained by the real sensors equipped in the current wind tunnel experiment.

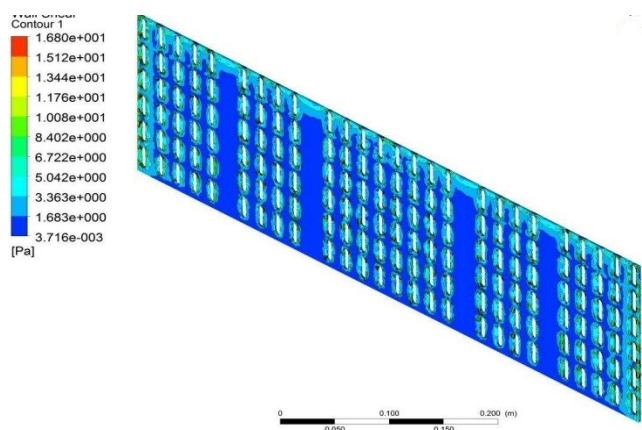


Figure 8. Contour of wall shear stress in porous zone

D. Position of the reattachment point

Reattachment point is determined by examining the horizontal velocity component at ground level to determine the point, where the horizontal velocity changes sign from upwind (negative) to downwind (positive) [1]. It is an important parameter to assess the shelter distance of a porous fence. It is unlikely to accurately capture a reattachment point under the current setup of wind tunnel experiment, since the sensor produced time averaged data that it is no possible to generate negative data.

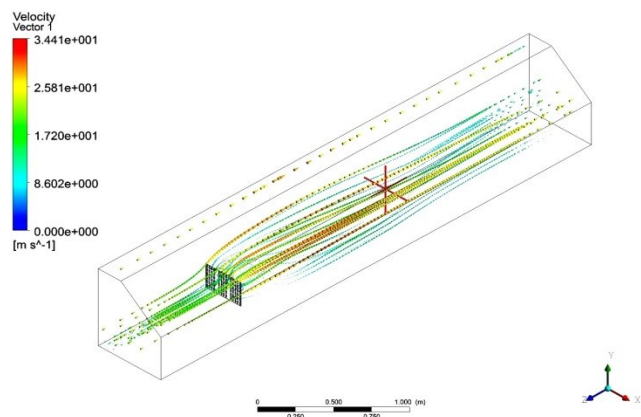


Figure 9. Reattachment point in the domain

In CFD simulation, as the time averaged bed shear stress reflects the velocity in the cell next to the boundary, then the reattachment is defined as the point where the near-wall velocity is zero. Therefore it can conveniently allocate the position of reattachment point in the domain. Figure 9 displays the red-cross is the position of the reattachment point, which is at $x, y, z = 3.1e-5, 0, -1668mm$.

E. Algorithmic outputs of CFD-based virtual sensor data

A power feature of CFD simulation is to generate algorithmic outputs of CFD-based virtual sensor data for analysis. It takes CFD generated data of dynamic head as an example, since dynamic head is a variable commonly used in the fluid dynamics research. Calculating dynamic head is based on the following formula:

$$q = \rho * (|u|)^2 / 2 \tag{4}$$

Where q is the dynamic head, ρ is the air density, and $|u|$ is the velocity magnitude.

In ANSYS Fluent, Using the Define command by opening the Custom Field Functions, the formula is easily to be written into the model. Figure 10. shows the contours of dynamic head in the symmetry wall.

CFD simulation can also generate its virtual sensor data by defining algorithm in its User Defined Functions. Outputs of data can be written to files by applying XY plot.

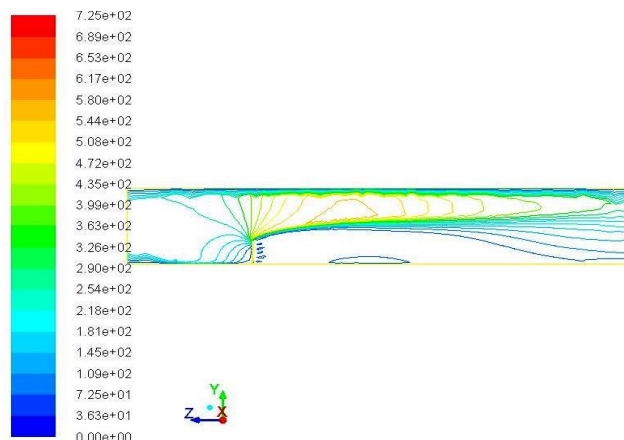


Figure 10. Contours of dynamic head

VI. CONCLUSIONS

In this paper, the CFD model has been assessed and its data of velocity magnitudes are in desirable agreement with the physical sensor data. Through an infinite number of virtual sensors, the model provides quantitative CFD-based virtual sensor data to comprehensively study the structure of air flow behind a porous fence. Comparing with physical experimental test, the CFD model has shown its strength with regard of flexibility, efficiency, relatively low cost and productivity. The model can be used in evaluating and designing porous fences.

It must be pointed out that CFD-based virtual sensor data are valid only after the model has been proved sound, which means that CFD modeling has to be examined and assessed by essential physical sensor data.

Future work on this research will apply this model for two-phase flow simulation (wind driven sediments like sands and snows).

ACKNOWLEDGEMENT

Norwegian Research Council financed this work under project number 195153 (ColdTech). The authors would also like to acknowledge the contribution of the industrial partner in this task: IKM dsc AS, Norway.

REFERENCES

- [1] Z. Dong, W. Luo, G. Qian, P. Lu and H. Wang, "A wind tunnel simulation of the mean velocity field behind upright porous wind fences," *Agricultural and Forest Meteorology*, vol. 146, pp. 82-93, 2007.
- [2] M. Jensen, Shelter effect: investigations into Aerodynamics of shelter and its effects on climate and crops, Copenhagen: Danish Tech. Press, 1954.
- [3] N. Tani, "On the wind tunnel test of the model shelter hedge," in *Bulletin of the Natinal Institute for Agricultural Sciences*, 1958.
- [4] J. Raine and D. Stevenson , "Wind protection by model fences in simulated atmospheric boundary layer," *Industrial Aerodynamics*, vol.

- 2, pp. 159-180, 1977.
- [5] S. Lee and H. Kim, "Laboratory measurements of velocity and turbulence field behind porous fences," *Wind. Eng. Ind. Aerodyn.*, vol. 80, pp. 311-326, 1999.
 - [6] L. Hagen and E. Skidmore, "Turbulent velocity fluctuations and vertical flow as affected by windbreak porosity," in *Trans.ASAE*, 1971A.
 - [7] J. Wilson, "Numerical studies of flow through a windbreak," *Wind Eng. Ind. Aerodyn.*, vol. 21, pp. 119-154, 1985.
 - [8] A. Packwood, "Flow through porous fences in thick boundary layers: comparisons between laboratory and numerical experiments," *Wind Eng. Ind. Aerodyn.*, vol. 88, pp. 75-90, 2000.
 - [9] S. Alhajraf, "Computational fluid dynamic modelling of drifting particles at porous fence," *Environmental Modelling and Software*, vol. 19, pp. 163-170, 2004.
 - [10] P. Bourdin and J. Wilson, "Windbreak aerodynamics: is computational fluid dynamics reliable?," *Boundary-Layer Meteorology*, vol. 126, pp. 181-208, 2008.
 - [11] E. Wilson, "Virtual sensor technology for process optimization," in *Symposium on Computers and Controls in the Metals Industry in Iron and Steel Society*, 1997.
 - [12] A. Jang, A. S. Man, J.-J. Kim, H. W. Choi, K. Hong, S. B. Lim, H. Kim and J.-H. Woo, "Implementation of CFD, sensor network, and distributed data management in support of micro-scale air quality management," in *6th International Conference on Computer Sciences and Convergence Information Technology (ICCIT)*, Seogwipo, 2011.
 - [13] Z. Sun and S. Wang, "A CFD-based test method for control of indoor environment and space ventilation," *Building and Environment*, vol. 45, pp. 1441-1447, 2010.
 - [14] B. Blocken, "50 years of Computational Wind Engineering: past, present and future," *Wind Engineering and Industrial Aerodynamics*, vol. 129, pp. 69-102, 2014.
 - [15] P. Richards and R. Hoxey, "Appropriate boundary conditions for computational wind engineering models using the k-e turbulence model," *Wind Eng. Ind. Aerodyn.*, vol. 46 (47), pp. 145-153, 1993.
 - [16] J. Wilson and C. Mooney, "A numerical simulation of boundary-layer flows near shelterbelts comments," *Boundary-Layer Meteorology*, vol. 85, pp. 137-149, 1997.
 - [17] J. Santiago, F. Martin, N. Bezdeneznykh and A. Sanz-Andres, "Experimental and numerical study of wind flow behind windbreaks," *Atmospheric Environ.*, vol. 41, pp. 6406-6420, 2007.
 - [18] N. Zhang, J.-H. Kang and S.-J. Lee, "Wind tunnel observation on the effect of a porous wind fence on shelter of saltating sand particles," *Geomorphology*, vol. 120, pp. 224-232, 2010.